

ARTICLE OPEN



Enhanced Arctic moisture transport toward Siberia in autumn revealed by tagged moisture transport model experiment

Tomonori Sato¹✉, Tetsu Nakamura^{1,4}, Yoshihiro Iijima² and Tetsuya Hiyama¹³

Rapid Arctic warming has altered the regional hydrological cycle through reduction in Arctic sea ice. Observational and modeling efforts provided evidence that the enhanced evaporation from the Arctic Ocean could increase snowfall over high latitude terrestrial zones. However, questions remain regarding the amount of equatorward moisture transport and its change over the decadal timescale. Here we show that the transport of atmospheric moisture to Siberia that originated from Arctic Ocean evaporation has increased significantly in autumn to early winter during 1981–2019 when substantial sea ice retreat was observed. The enhanced Arctic moisture content is found in western Siberia in September, consistent with the observed increase in snow cover investigated in earlier studies. Meanwhile, the annual maximum daily amount of Arctic moisture shows a sharp increase in eastern Siberia during October–December associated with cyclonic activities along coastal regions. Our results suggest the importance of monitoring equatorward moisture transport during snow accumulation seasons because it could enhance local snowstorms as evaporation from the Arctic Ocean increases in the near future.

npj Climate and Atmospheric Science (2022)5:91; <https://doi.org/10.1038/s41612-022-00310-1>

INTRODUCTION

There is growing concern in relation to the influence of climate change on the natural environment and on human socioeconomic activities. The impacts of climate change extend globally but with substantial inhomogeneity. Among Earth's various environmental systems, those that exist in the Arctic and circum-Arctic regions have been affected strongly by rapid warming, which is projected to continue at a rate approximately twice that of the global mean¹. The enhanced warming in the Arctic region, referred to as Arctic amplification, is not simply a local issue because it weakens the latitudinal thermal gradient, causing jet meandering that could possibly trigger abnormal weather in mid-latitude regions². The accelerated warming in the Arctic is maintained by complex interactive processes that encompass components of the ocean, land, and atmosphere. In such interactions, the hydrological cycle plays a focal role by regulating ice–albedo feedback and radiative energy transfer³.

The issues that remain unexplained with respect to the hydrological cycle include the effect of Arctic warming on continental snowfall. During seasonal transitions, snow cover predominantly regulates the surface energy budget. Many earlier studies demonstrated that snow cover exerts a memory effect in which the signal of a hydrometeorological episode is stored as a snow cover anomaly during the cold season, and that this signal re-emerges several months later during the snowmelt season to reinforce the atmosphere^{4,5}. Therefore, knowledge of a precursor signal stored as a snow cover anomaly is expected to help improve seasonal prediction of abnormal weather, e.g., the potential for modulation of the likelihood of heatwaves^{6,7} that enhance the risk of fire in boreal forests^{8,9}.

The recent rapid reduction in Arctic sea ice and evident warming of the Arctic Ocean are likely to increase snow cover over northern Eurasia^{10–12}. It was revealed that heavy snowfall events over Europe are attributable to atmospheric moisture supplied

from the Barents Sea, and that such a mechanism explains the decadal change in snowfall over the Scandinavian Peninsula¹². It is reasonable to hypothesize that similar pathways of equatorward moisture transport exist across northern Siberia where the distance from the low- and mid-latitude oceans is large. An idealized general circulation model experiment predicted that an ice-free Arctic Ocean would increase the extent of snow cover over Siberia¹⁰. A Lagrangian moisture transport model showed consistent results, whereby the airmass over the Arctic Ocean acquires more humidity in years with low ice cover, which increases precipitation over western Siberia¹¹. Despite these earlier efforts, questions remain regarding the amount of equatorward moisture transport that originates from the Arctic Ocean and its change over the decadal timescale. Therefore, the objective of this study was to quantify the fraction of water vapor evaporated from the Arctic Ocean, and to investigate its transport to northern Eurasia, particularly Siberia, during recent decades when Arctic sea ice retreat has been remarkable. The analysis was conducted using a tagged moisture transport model ("Methods"). Because the model was driven using a reanalysis dataset, we attempted to diagnose the reality of the effects of the moisture released from the Arctic Ocean.

RESULTS

Distribution of Arctic moisture along coastal Siberia

The simulation was performed for the period 1981–2019. This study focused on the transport of moisture evaporated from the Arctic Ocean (area colored navy blue in Fig. 1). Figure 2 illustrates a longitude–time cross-section of the mass amount of atmospheric water vapor evaporated from the Arctic Ocean (hereafter, Arctic moisture). The cross section was aligned to traverse coastal inland regions of the northern fringe of Eurasia to ensure monitoring of the advection of Arctic moisture into Siberia (Fig. 1). It can be seen

¹Faculty of Environmental Earth Science, Hokkaido University, Sapporo, Japan. ²Graduate School of Bioresources, Mie University, Tsu, Japan. ³Institute for Space-Earth Environmental Research, Nagoya University, Nagoya, Japan. ⁴Present address: Climate Prediction Division, Japan Meteorological Agency, Tokyo, Japan.
✉email: t_sato@ees.hokudai.ac.jp

that there is a clear seasonal transition in precipitable water vapor (PWV) from the wet summers to the dry winters. In all months, Arctic moisture shows large equatorward transport over western parts of Siberia, with a clear division at around 90°E that corresponds to the location of the Ural Mountains (Fig. 2). This longitudinal distribution of Arctic moisture largely reflects the terrain height, which determines the attainable amount of water vapor content, i.e., saturation precipitable water. Another reason

will be the spatial inhomogeneity of the distribution of Arctic sea ice. The western side of the cross section lies close to the Barents–Kara seas where the sea ice fraction is low throughout the year. In contrast, the eastern side lies close to the Laptev and East Siberian seas that have sporadic sea ice cover.

The years with high concentration of Arctic moisture in August broadly correspond to those years with strong southward moisture transport (Fig. 2). Southward moisture flux over western Siberia in August appears dominant after around 1995, consistent with the development of the mid-tropospheric trough in this region^{13,14}. In September, the monthly mean concentration of Arctic moisture over western Siberia exceeds 3.0 mm in many years, although large interannual variation exists (Fig. 2). There is a sharp drop in PWV after September in eastern Siberia. An interesting characteristic evident in October and November is the relatively high Arctic moisture in some years over eastern Siberia (Supplementary Fig. 1), which is discussed later. The cross sections shown in Fig. 2 and Supplementary Fig. 1 indicate that a large amount of water vapor evaporated from the Arctic Ocean is transported to northern Eurasia, and that its magnitude has increased in recent decades during autumn to early winter.

Interannual variation of Arctic moisture and the driving circulation

Figure 3 shows the spatial distribution of the linear trend of the amount of Arctic moisture during autumn to early winter (September–December). The Arctic Ocean area mostly shows a strong positive trend, which means that, in conjunction with poleward moisture transport from other source regions¹⁵, the water vapor supplied from the underlying ocean has increased significantly since the early 1980s. This increasing trend forms an annular pattern centered around the North Pole, except over Greenland where the trend is insignificant. This suggests that the

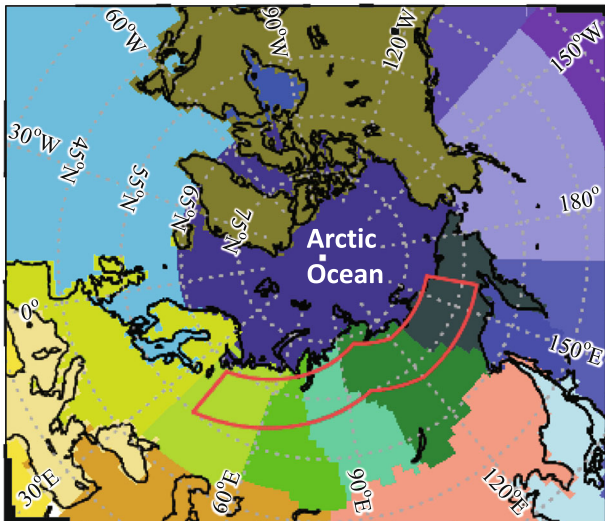


Fig. 1 Definition of moisture source regions. Colors are assigned to regions where evaporated water is investigated. The Arctic Ocean is colored navy blue. The red line denotes the area used for the cross section shown in Fig. 2.

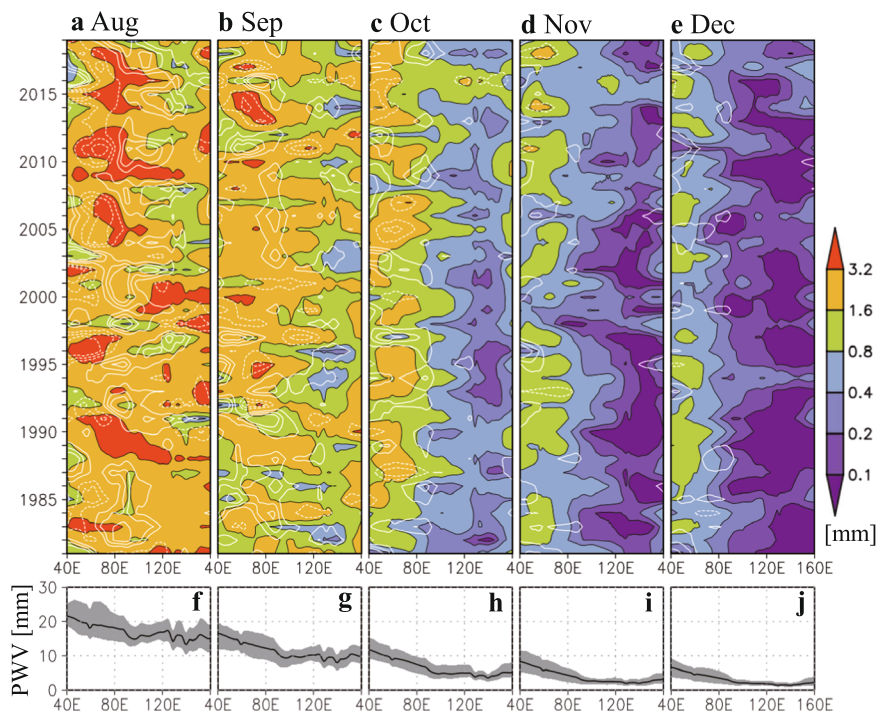


Fig. 2 Distribution of water vapor evaporated from Arctic Ocean. **a–e** Longitude–time cross section of monthly mean water vapor amount evaporated from the Arctic Ocean (shading; mm) averaged along the coastal inland area (see Fig. 1). Contours indicate meridional component of water vapor flux including all moisture sources. Contour interval is $20 \text{ kg m}^{-2} \text{ s}^{-1}$ (omitting zero), and the solid and dashed lines represents poleward and equatorward transport, respectively. **f–j** Longitudinal distribution of climatological (1981–2019) monthly averaged precipitable water vapor (mm). Shading denotes highest and lowest values during the study period.

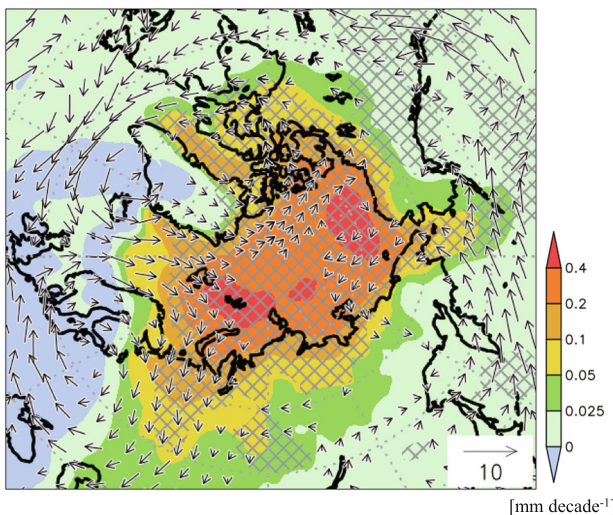


Fig. 3 Trend of Arctic moisture during September–December. Spatial distribution of the linear trends in Arctic moisture (mm decade^{-1}) and water vapor flux ($\text{kg m}^{-1} \text{s}^{-1} \text{decade}^{-1}$) during September–December, omitting values <1.0 . The water vapor flux is for the accumulation of all moisture sources. Hatching denotes a trend statistically significant at the 95% confidence level.

water vapor evaporated from the Arctic Ocean, which is likely due to the increase in sea surface temperature and widened ice-free area, is confined mainly within the Arctic oceanic atmosphere. The areas with significant increase in Arctic moisture content expands toward extrapolar regions such as northern Eurasia, the North Pacific, and North America, but the magnitude of the trend decreases rapidly with increasing distance from the Arctic Ocean. Pronounced southward extension of Arctic moisture is found over western Siberia, Bering Strait, and the region from northeastern Canada to Baffin Bay. The increased concentration in western Siberia accompanies intensification of the southward moisture flux that traverses the Barents Sea as part of the clockwise circulation centered over the Scandinavian Peninsula.

There is prominent monthly variation in the linear trend of Arctic moisture over northern Eurasia. Figure 4 compares the trend for each month from autumn to early winter. The spatial distribution of the trend in September (Fig. 4a) resembles that of the seasonal mean (Fig. 3). This reflects the larger magnitude of the trend in September than in the following months (Fig. 2) and increased concentration of Arctic moisture over the northern Barents Sea (Fig. 3). A strong trend of increase in Arctic moisture is found in eastern Siberia during October–December. This is consistent with increased evaporation over the East Siberian Sea and the Chukchi Sea in October, which is probably the result of local sea ice retreat and ocean warming (Fig. 4b–d). Indeed, the area with increased evaporation coincides where sea ice has been replaced with open ocean during the study period rather than the area with SST warming (Supplementary Fig. 2) in consistent with previous studies¹⁶. In contrast, the evaporation change is relatively small in other parts of Arctic Ocean. This is likely attributable to the humidification of the airmass lying above the ocean¹⁷.

To investigate recent changes in major moisture transport events, daily analysis was performed. The maximum daily concentration of Arctic moisture identified for each year shows increasing trend in September that extends widely over Siberia, but it is not statistically significant except coastal regions in western Siberia (Fig. 4e). This implies that the daily extreme events are likely to have contributed to the increasing trend in Fig. 4a but are not only factor. In contrast, a significant trend of increase is found over both the Lena River basin and northeastern Siberia during October–December (Fig. 4f–h). The similarity between the

trend patterns for monthly average values and maximum daily values during October–December indicates that the trend of increase in Arctic moisture is attributable to the occurrence of extreme moisture transport events. Indeed, the magnitude of the trend (maximum daily value: $\sim 0.4\text{--}0.8 \text{ mm decade}^{-1}$) is approximately four times greater than the trend for the monthly average value, suggesting that moisture transport on particular days is substantial. The fields of monthly average horizontal water vapor flux during October–December can reasonably explain how moisture is transported, but they appear insufficiently weak, especially in inland regions. Hence, the following analysis focuses on the events that accompanied strong equatorward transport of Arctic moisture.

Figure 5 shows interannual variations of the maximum values of daily Arctic moisture content. Here, the targeted areas were selected to cover the regions showing increasing trends in Fig. 4 (i.e., western Siberia for September and eastern Siberia for October–December). Over western Siberia, Arctic moisture in September shows a clear increase with large interannual variation after the late 2000s. Because the sea ice fraction over the neighboring ocean (i.e., the Barents and Kara seas) was not abnormally low in these years, the high fraction of Arctic moisture was presumably maintained by circulation anomalies in these years rather than by increased evaporation (not shown). Such landward moisture transport from the Arctic Ocean might contribute to enhanced snow cover over western Siberia, as reported by observational studies¹⁸. Moisture advection from the Arctic Ocean typically occurs under northerly winds, which also bring low-temperature polar air. Thus, it can establish atmospheric conditions favorable for snowfall. Similarly, an enhanced fraction of Arctic moisture is obvious in eastern Siberia during October–December after around 2005 (Fig. 5b–d). Interestingly, the estimated amount of maximum daily precipitation composed of Arctic moisture tends to show a similar interannual variation with that of PWV (Fig. 5b–d). This result reveals that events with high Arctic moisture coincide with precipitation events, and that they have influenced snowfall in eastern Siberia. Such recent enhancement of the transport of Arctic moisture appears associated with the circulation patterns that cause heavy snowfall over Siberia during autumn to early winter¹⁹. Further investigation of the moisture source associated with heavy snowfall events over eastern Siberia is urgently needed.

Supplementary Fig. 3 depicts the interannual variation of precipitable water vapor and its origin in the day of maximum Arctic moisture. In both October and November, the proportion of Arctic moisture against total precipitable water exhibits large interannual variation (3–58%). The local terrestrial evaporation from Siberian regions is more dominant than the Arctic moisture in the inland Siberia. In November, however, statistically significant increase ($p < 0.05$) is detected only for Arctic moisture. Interestingly, the increased Arctic moisture in recent decades appears to contribute increased total precipitable water. Given that water vapor act as strong greenhouse gas, the enhanced moisture content originated from the Arctic Ocean may have influence on the radiation balance and the enhanced warming in the inland areas of eastern Siberia. Besides, the figure shows relatively large fraction of water vapor originated from the Siberian regions. Temporal variation of terrestrial evapotranspiration could also lead to important contribution to circum-Arctic hydrological cycle.

DISCUSSION

Our modeling approach provides insight into the source–receptor relationship of moisture transport from the Arctic Ocean to Siberia. The results show that the amount of atmospheric moisture reaching Siberia that originated from the Arctic Ocean has increased in recent decades. Such a flow of moisture is in the opposite direction to the climatological moisture flow (i.e., poleward), which is maintained by

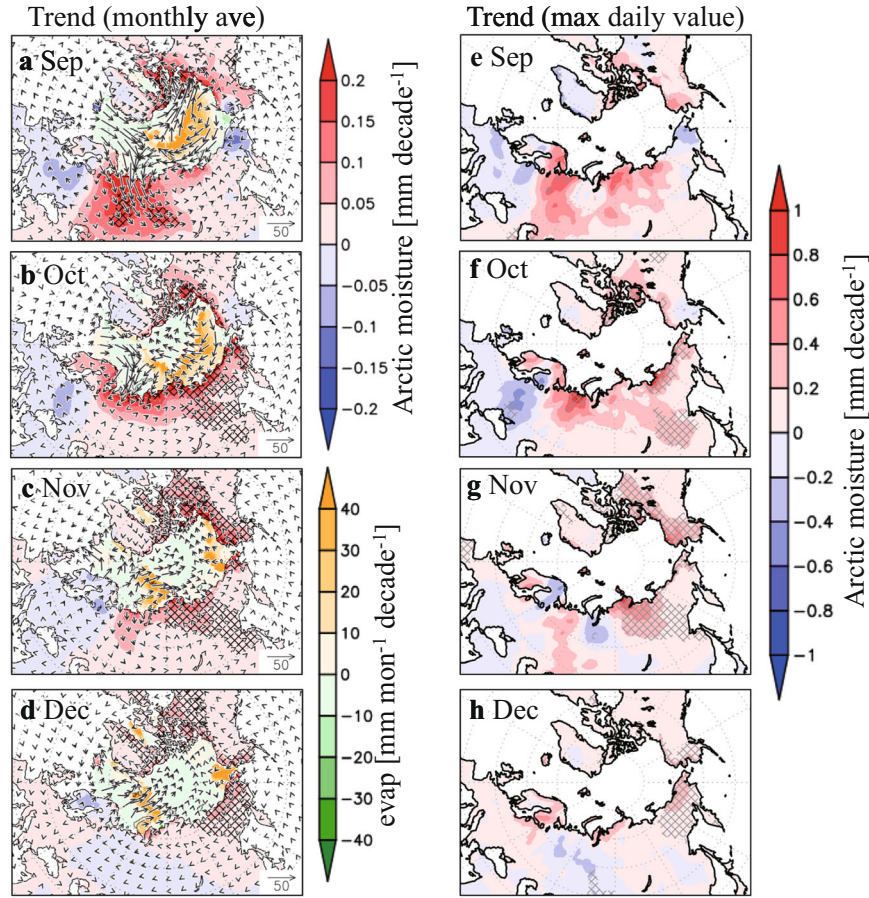


Fig. 4 Trend of monthly-mean Arctic moisture. **a–d** Linear trends of Arctic moisture for each month (shading over land; mm decade^{-1}) and evaporation (shading over the Arctic Ocean; $\text{mm month}^{-1} \text{decade}^{-1}$). Vectors are as described in Fig. 3 but for each month. **e–h** Linear trends of daily Arctic moisture content in terms of their highest value in each year (mm decade^{-1}). Hatching denotes a trend significant at the 95% confidence level.

the mean-state latitudinal gradient of atmospheric moisture content (i.e., drying toward the pole). To better understand the circulation pattern attributable to the recent increase in the fraction of Arctic moisture, we discuss the synoptic fields relevant to the periods in which strong moisture transport was detected.

Figure 6 shows the daily evolution of the synoptic patterns in advance of the day on which the highest amount of Arctic moisture over eastern Siberia was observed in October ($60^{\circ}\text{--}70^{\circ}\text{N}$, $130^{\circ}\text{--}150^{\circ}\text{E}$) and November ($60^{\circ}\text{--}70^{\circ}\text{N}$, $110^{\circ}\text{--}130^{\circ}\text{E}$). From September 27 to October 1, 2016, a cut-off low centered over northeastern Siberia migrated northeastward (Fig. 6a–c). The counterclockwise circulation around the low strengthened the surface winds over the East Siberian Sea where sea ice was absent (Supplementary Fig. 4a–c). Thus, an air mass with high content of Arctic moisture, created there through evaporation from the ocean, was transported toward Siberia owing to the northerly winds on the western side of the low. Another event with high Arctic moisture occurred on November 18, 2016 (Fig. 6d–f). This case was characterized by a strong northerly wind between an area of low pressure centered around the Sea of Okhotsk and eastern Siberia and an area of high pressure over western Siberia (Fig. 6f). This synoptic situation resembles the pattern designated as Ural blocking, which has received considerable attention regarding Arctic amplification^{20,21}. Before the development of these circulation anomalies, a westerly wind prevailed in parallel with the coastlines of the Barents–Kara seas, which supported the transport of air with high content of Arctic moisture (Fig. 6d, e). There was an ice-free and warm ocean under the region of the

westerly wind (Supplementary Fig. 4d–f), which promoted evaporation from the Arctic Ocean. Finally, strong northerly winds pushed the Arctic moisture into central and eastern Siberia on November 18, 2016 (Fig. 6f).

The above two case studies highlight the importance of an ice-free ocean, but they also demonstrate that the moisture pathway can be case-dependent. The common feature of these cases is the presence of cyclonic/anticyclonic systems that strengthened equatorward winds in the lower troposphere. Earlier studies revealed that the presence of strong poleward moisture transport partly helps maintain Arctic warming^{22–24}. Because cyclonic and anticyclonic systems enhance both poleward and equatorward winds, they can induce strong poleward and Arctic-to-Siberia moisture transport simultaneously. The latter component will become increasingly important as the extent of Arctic sea ice diminishes and evaporation from the ocean increases. Latent heat flux from the Arctic Ocean becomes high during autumn to early winter, which is when low sea ice coverage and high sea surface temperature are expected. Future studies should be devoted to linking the changes in evaporation, atmospheric moisture transport, and storm track along the coastal regions of the Arctic Ocean in this season. Monitoring of the behavior of Arctic moisture should be important for studies related to heavy snowstorms in circumpolar regions because southward moisture transport is likely to accompany cold air outbreaks from the polar airmass.

The boreal ecosystem that lies over northern parts of Eurasia has a crucial function as a huge carbon stock in the Earth climate system. Extreme precipitation events in autumn could accelerate

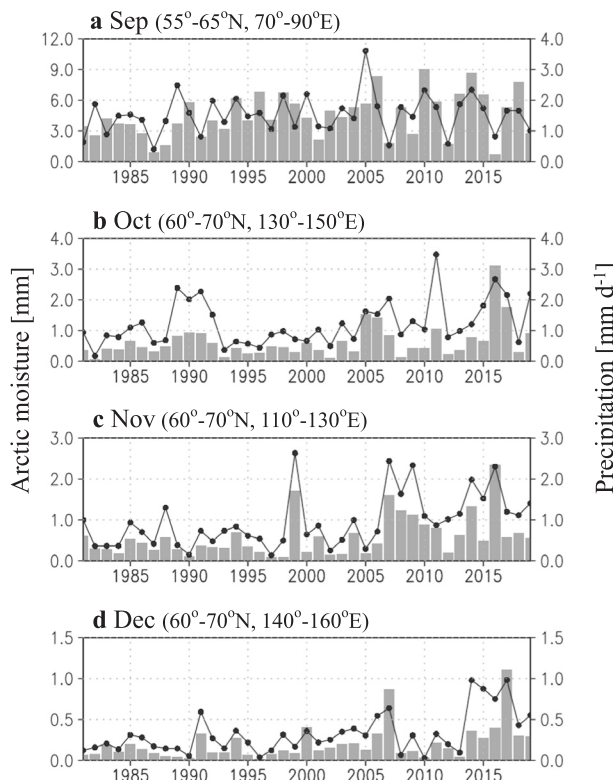


Fig. 5 Historical changes of Arctic moisture. Interannual variations of maximum daily Arctic moisture content (bar and left axis, mm) and fraction of precipitation originated from the Arctic Ocean (line and right axis, mm day^{-1}) averaged over **a** western Siberia in September and **b-d** eastern Siberia during October–December. The domain used for area averaging is indicated in each panel. The precipitation fraction was computed by assuming that the rate of Arctic moisture against precipitable water vapor is also retained for precipitation.

the deepening of the active layer in permafrost regions²⁵. Permafrost degradation could enhance global warming through a combination of feedback processes that involve net emission of greenhouse gases through release of methane and possible reduction of photosynthesis owing to the occurrence of forest fires^{26,27}. A change in winter snow cover affects ecohydrological systems in the following summer through alteration of water availability and thermal conditions^{28,29}. Therefore, terrestrial ecosystems in circumpolar regions are highly sensitive to atmospheric and surface hydrological cycles during the snow-accumulation period. This study demonstrated that atmospheric moisture evaporated from the Arctic Ocean is transported to Siberia, and that its amount has increased during autumn to early winter. It is suggested that this increase is driven partly by cyclonic activity around the coastal regions of northern Siberia and by expansion of the ice-free ocean area. Further analysis will be essential to elucidate how these changes might contribute to the characteristics of snow over Siberia. Moreover, interdisciplinary studies should be conducted to evaluate the possible influences of Arctic moisture transport on the terrestrial environment.

METHODS

Moisture transport model

This study developed a tagged moisture transport model based on the atmospheric moisture balance. The water vapor tracer schemes have been implemented in general circulation models^{30–32}, which have demonstrated capability in tracing a specific

component of the water vapor that circulates within atmospheric and surface hydrological cycles. The results can be validated using in situ measurements or remote sensing of stable isotopes³³. A possible caveat regarding this approach is that the simulated dynamic and thermodynamic atmospheric fields are not identical to their actual daily variations in the past, except for short-term case studies with initialization^{34,35} or experiments with strong nudging³⁶. Hence, previous application of tagged moisture analysis to climate studies has been limited. In climate studies, the gap between the simulated and the real atmosphere is expected to become greater with increasing distance from the ocean toward inland areas because nonlinear land–atmosphere interactions become predominant in determining the hydrological cycle. To overcome this problem, we adopted a tagged moisture transport model driven using a reanalysis product as the forcing data. This approach enables simulation under real hydrological cycle conditions that reflect the observed atmospheric circulation and the observed changes in surface properties such as sea surface temperature, sea ice, and terrestrial ecosystems initialized with reasonably realistic settings.

The basic concept of the model, which follows previous studies^{37,38}, is summarized below. A prognostic equation of precipitable water vapor (PWV) is described as

$$\frac{d\text{PWV}}{dt} = \text{EPT} + \text{CONV} - \text{PRCP} \quad (1)$$

where EPT, CONV, and PRCP represent evapotranspiration, convergence of column-integrated atmospheric water vapor, and precipitation, respectively. The fraction of the tagged moisture component also satisfies the water balance. Representing each moisture source region as subscript n and the total number of source regions as N , Eq. (1) can be rewritten as follows:

$$d\text{PWV}_n = \text{EPT}_n + \text{CONV}_n - \text{PRCP}_n \text{ where } n = 1, 2, \dots, N \quad (2)$$

$$\text{PWV} = \sum_{n=1}^N \text{PWV}_n \quad (3)$$

Applying the reanalysis dataset to constrain the spatial distributions of PWV, EPT, CONV, and PRCP at any arbitrary time, we can predict PWV _{n} at any location.

As described in Eqs. (1) and (2), the model predicts the moisture budget for the column air. Thus, the vertical variation of moisture source composition is not considered. This is mainly because of the limitation in simulating subgrid processes that regulate vertical moisture transport, such as turbulent eddy transport and convective updraft/downdraft that often accompanies with phase change of water. To incorporate these processes in the moisture tracer modeling, parameterization schemes will be required. Modern GCMs with moisture tracers have implemented these processes³⁹, but the simulated hydrological cycle, in particular for precipitation, contains model bias. The bias tends to cause discrepancy in stable isotope ratios between the model and observations³⁷. It was found that two-dimensional horizontal moisture transport is the main driver of the stable isotope variations at the daily scale³⁹. Similar two-dimensional approach succeeded in simulating observed isotope variation in high-latitude Eurasia³⁸, and their moisture source analysis performed a good resemblance to the GCM simulation³². These evidences generally support the methodology of current study has sufficient reliability in simulating the behavior of Arctic moisture.

Experiment and data

This study used the Japanese 55-year reanalysis dataset (JRA-55)⁴⁰. The simulation for the period 1981–2019 was conducted with a 1-h time step and $1.25^\circ \times 1.25^\circ$ horizontal resolution. The hourly fields of the variables were created through linear interpolation of

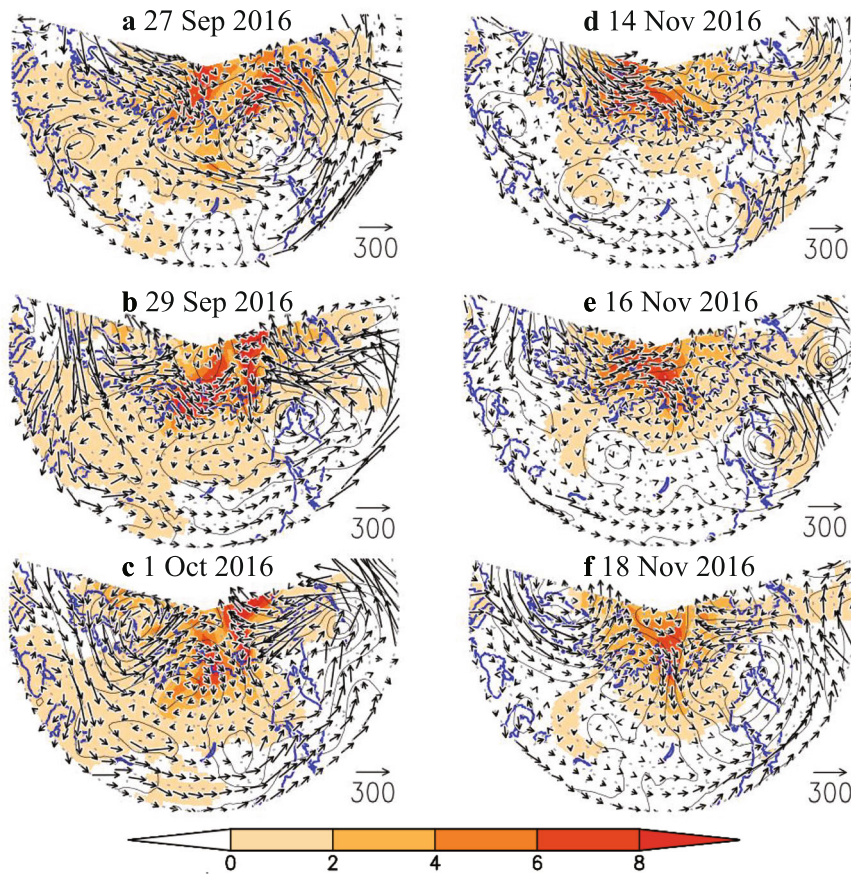


Fig. 6 Pathways of Arctic moisture. Geopotential height at 850 hPa (contour, m) with 60-m intervals and column-integrated water vapor flux (vector, $\text{kg m}^{-1} \text{s}^{-1}$) during events of high transportation of Arctic moisture. Shading illustrates the distribution of Arctic moisture (mm). **a–c** September 27 to October 1, 2016; **d–f** November 14–18, 2016.

the JRA-55's 3-h dataset. Because evapotranspiration and precipitation are not subjected to data assimilation and are instead derived from the model forecast in the data assimilation cycle, bias correction was performed prior to the simulation. The bias of these variables at each grid point was corrected to have the same monthly climatological values as the independent reference dataset according to Eq. (4):

$$A(t)_{\text{corrected}} = A(t)_{\text{reanalysis}} \times \frac{\langle A_{\text{reference}} \rangle_{\text{Mon}=i}}{\langle A_{\text{reanalysis}} \rangle_{\text{Mon}=i}} \quad i = 1, \dots, 12 \quad (4)$$

where $A(t)$ represents the hourly interval variables to be corrected and $\langle \cdot \rangle_{\text{Mon}=i}$ represents their climatological mean for month i . The reference datasets for evapotranspiration and precipitation were the Continuous Satellite-derived Global Record of Monthly Land Surface Evapotranspiration⁴¹ (averaged over 1983–2006), provided by ORNL DAAC, and the GPCP v2.2 combined⁴² (averaged over 1981–2010), provided by NOAA/OAR/ESRL PSD, respectively. The definition of moisture source regions is illustrated in Fig. 1. This study focused on the transport of moisture evaporated from the Arctic Ocean (area colored navy blue in Fig. 1).

DATA AVAILABILITY

JRA-55 reanalysis dataset is available at https://jra.kishou.go.jp/JRA-55/index_en.html. The reference datasets used for bias correction are available at http://webmap.ornl.gov/ogcdown/dataset.jsp?ds_id=10020 and <http://www.esrl.noaa.gov/psd/data/gridded/data.gpcp.htm>.

CODE AVAILABILITY

All codes used for analyses are developed by the corresponding author and available upon reasonable request.

Received: 1 April 2022; Accepted: 12 October 2022;

Published online: 24 November 2022

REFERENCES

- IPCC. in *Climate Change 2021: The Physical Science Basis. Contribution of Working Group I to the Sixth Assessment Report of the Intergovernmental Panel on Climate Change* (eds Masson-Delmotte, V. et al.) (Cambridge University Press, 2021).
- Coumou, D., Di Capua, G., Vavrus, S., Wang, L. & Wang, S. The influence of Arctic amplification on mid-latitude summer circulation. *Nat. Commun.* **9**, 1–12 (2018).
- Dai, A., Luo, D., Song, M. & Liu, J. Arctic amplification is caused by sea-ice loss under increasing CO_2 . *Nat. Commun.* **10**, 1–13 (2019).
- Matsuura, S., Yamazaki, K. & Sato, T. Role of Siberian land-atmosphere coupling in the development of the August Okhotsk high in 2008. *J. Meteor. Soc. Jpn.* **93**, 229–244 (2015).
- Nakamura, T., Yamazaki, K., Sato, T. & Ukita, J. Memory effects of Eurasian land processes cause enhanced cooling in response to sea ice loss. *Nat. Commun.* **10**, 1–8 (2019).
- Sato, T. & Nakamura, T. Intensification of hot Eurasian summers by climate change and land–atmosphere interactions. *Sci. Rep.* **9**, 1–8 (2019).
- Nakamura, T. & Sato, T. A possible linkage of Eurasian heat wave and East Asian heavy rainfall in relation to the rapid Arctic warming. *Environ. Res.* **209**, 112881 (2022).
- Yasunari, T. J. et al. Extreme air pollution events in Hokkaido, Japan, traced back to early snowmelt and large-scale wildfires over East Eurasia: case studies. *Sci. Rep.* **8**, 1–10 (2018).

9. Yasunari, T. J. et al. Relationship between circum-Arctic atmospheric wave patterns and large-scale wildfires in boreal summer. *Environ. Res. Lett.* **16**, 064009 (2021).
10. Ghatak, D. et al. Simulated Siberian snow cover response to observed Arctic sea ice loss, 1979–2008. *J. Geophys. Res. Atmos.* <https://doi.org/10.1029/2012JD018047> (2012).
11. Wegmann, M. et al. Arctic moisture source for Eurasian snow cover variations in autumn. *Environ. Res. Lett.* **10**, 054015 (2015).
12. Bailey, H. et al. Arctic sea-ice loss fuels extreme European snowfall. *Nat. Geosci.* **14**, 283–288 (2021).
13. Erdenebat, E. & Sato, T. Recent increase in heat wave frequency around Mongolia: role of atmospheric forcing and possible influence of soil moisture deficit. *Atmos. Sci. Lett.* **17**, 135–140 (2016).
14. Piao, J., Chen, W. & Chen, S. Water vapour transport changes associated with the interdecadal decrease in the summer rainfall over Northeast Asia around the late-1990s. *Int. J. Climatol.* **41**, E1469–E1482 (2021).
15. Rinke, A. et al. Trends of vertically integrated water vapor over the Arctic during 1979–2016: consistent moistening all over? *J. Clim.* **32**, 6097–6116 (2019).
16. Nygård, T., Naakka, T. & Vihma, T. Horizontal moisture transport dominates the regional moistening patterns in the Arctic. *J. Clim.* **33**, 6793–6807 (2020).
17. Vihma, T. et al. The atmospheric role in the Arctic water cycle: a review on processes, past and future changes, and their impacts. *J. Geophys. Res. Biogeosci.* **121**, 586–620 (2016).
18. Bulygina, O. N., Razuvayev, V. N. & Korshunova, N. N. Changes in snow cover over Northern Eurasia in the last few decades. *Environ. Res. Lett.* **4**, 045026 (2009).
19. Bednorz, E. & Wibig, J. Circulation patterns governing October snowfalls in southern Siberia. *Theor. Appl. Climatol.* **128**, 129–139 (2017).
20. Luo, D. et al. Impact of Ural blocking on winter warm Arctic–cold Eurasian anomalies. Part I: Blocking-induced amplification. *J. Clim.* **29**, 3925–3947 (2016).
21. Yao, Y., Luo, D., Dai, A. & Simmonds, I. Increased quasi stationarity and persistence of winter Ural blocking and Eurasian extreme cold events in response to Arctic warming. Part I: Insights from observational analyses. *J. Clim.* **30**, 3549–3568 (2017).
22. Gong, T. & Luo, D. Ural blocking as an amplifier of the Arctic sea ice decline in winter. *J. Clim.* **30**, 2639–2654 (2017).
23. Rinke, A. et al. Extreme cyclone events in the Arctic: wintertime variability and trends. *Environ. Res. Lett.* **12**, 094006 (2017).
24. Komatsu, K. K., Alexeev, V. A., Repina, I. A. & Tachibana, Y. Poleward upgliding Siberian atmospheric rivers over sea ice heat up Arctic upper air. *Sci. Rep.* **8**, 1–15 (2018).
25. Iijima, Y., Nakamura, T., Park, H., Tachibana, Y. & Fedorov, A. N. Enhancement of Arctic storm activity in relation to permafrost degradation in eastern Siberia. *Int. J. Climatol.* **36**, 4265–4275 (2016).
26. Meredith, M. et al. in *IPCC Special Report on the Ocean and Cryosphere in a Changing Climate* (eds Pörtner, H.-O. et al.) (IPCC, 2019).
27. Natali, S. M. et al. Permafrost carbon feedbacks threaten global climate goals. *Proc. Natl Acad. Sci. USA* <https://doi.org/10.1073/pnas.2100163118> (2021).
28. Grippa, M. et al. The impact of snow depth and snowmelt on the vegetation variability over central Siberia. *Geophys. Res. Lett.* <https://doi.org/10.1029/2005GL024286> (2005).
29. Suzuki, K. et al. Accelerated continental-scale snowmelt and ecohydrological impacts in the four largest Siberian river basins in response to spring warming. *Hydrolog. Process.* **34**, 3867–3881 (2020).
30. Bosilovich, M. G. & Schubert, S. D. Water vapor tracers as diagnostics of the regional hydrologic cycle. *J. Hydrometeorol.* **3**, 149–165 (2002).
31. Yoshimura, K., Kanamitsu, M., Noone, D. & Oki, T. Historical isotope simulation using reanalysis atmospheric data. *J. Geophys. Res. Atmos.* <https://doi.org/10.1029/2008JD010074> (2008).
32. Piao, J., Chen, W., Chen, S., Gong, H. & Zhang, Q. Summer water vapor sources in Northeast Asia and East Siberia revealed by a moisture-tracing atmospheric model. *J. Clim.* **33**, 3883–3899 (2020).
33. Yoshimura, K. Stable water isotopes in climatology, meteorology, and hydrology: a review. *J. Meteor. Soc. Jpn.* **93**, 513–533 (2015).
34. Tanoue, M., Ichiyangai, K., Yoshimura, K., Shimada, J. & Hirabayashi, Y. Estimation of the isotopic composition and origins of winter precipitation over Japan using a regional isotope circulation model. *J. Geophys. Res. Atmos.* **122**, 11621–11637 (2017).
35. Li, X., Kawamura, R., Sugimoto, A. & Yoshimura, K. Estimation of water origins within an explosive cyclone over the Sea of Japan using an isotopic regional spectral model. *J. Hydrometeorol.* **22**, 2825–2841 (2021).
36. Yoshimura, K. & Kanamitsu, M. Dynamical global downscaling of global reanalysis. *Monit. Weather Rev.* **136**, 2983–2998 (2008).
37. Yoshimura, K., Oki, T. & Ichiyangai, K. Evaluation of two-dimensional atmospheric water circulation fields in reanalyses by using precipitation isotopes databases. *J. Geophys. Res. Atmos.* <https://doi.org/10.1029/2004JD004764> (2004).
38. Sato, T. et al. Water sources in semi-arid Northeast Asia as revealed by field observations and isotope transport model. *J. Geophys. Res. Atmos.* **112**, D17112 (2007).
39. Yoshimura, K., Oki, T., Ohte, N. & Kanae, S. A quantitative analysis of short-term ^{18}O variability with a Rayleigh-type isotope circulation model. *J. Geophys. Res. Atmos.* <https://doi.org/10.1029/2003JD003477> (2003).
40. Kobayashi, S. et al. The JRA-55 reanalysis: general specifications and basic characteristics. *J. Meteor. Soc. Jpn.* **93**, 5–48 (2015).
41. Zhang, K., Kimball, J. S., Nemani, R. R. & Running, S. W. A continuous satellite-derived global record of land surface evapotranspiration from 1983 to 2006. *Water Resour. Res.* **46**, W09522 (2010).
42. Adler, R. F. et al. The Version 2 Global Precipitation Climatology Project (GPCP) monthly precipitation analysis (1979–present). *J. Hydrometeorol.* **4**, 1147–1167 (2003).

ACKNOWLEDGEMENTS

This study was supported by the Japan Society for the Promotion of Science KAKENHI (Grant Number: JP19H05668), the Arctic Challenge for Sustainability II (ArCSII) project (Grant Number: JPMXD1420318865), and JST SICORP (Grant Number: JPMJSC1902), Japan. We thank James Buxton, MSc, from Edanz (<https://jp.edanz.com/ac>) for editing a draft of this manuscript.

AUTHOR CONTRIBUTIONS

T.S. and T.H. designed the research and T.S. developed the model and performed the numerical experiments and analysis. T.N. advised the analysis and interpretation of the results. T.S. wrote the original manuscript and T.N., Y.I., and T.H. helped revise the manuscript.

COMPETING INTERESTS

The authors declare no competing interests.

ADDITIONAL INFORMATION

Supplementary information The online version contains supplementary material available at <https://doi.org/10.1038/s41612-022-00310-1>.

Correspondence and requests for materials should be addressed to Tomonori Sato.

Reprints and permission information is available at <http://www.nature.com/reprints>

Publisher's note Springer Nature remains neutral with regard to jurisdictional claims in published maps and institutional affiliations.



Open Access This article is licensed under a Creative Commons Attribution 4.0 International License, which permits use, sharing, adaptation, distribution and reproduction in any medium or format, as long as you give appropriate credit to the original author(s) and the source, provide a link to the Creative Commons license, and indicate if changes were made. The images or other third party material in this article are included in the article's Creative Commons license, unless indicated otherwise in a credit line to the material. If material is not included in the article's Creative Commons license and your intended use is not permitted by statutory regulation or exceeds the permitted use, you will need to obtain permission directly from the copyright holder. To view a copy of this license, visit <http://creativecommons.org/licenses/by/4.0/>.

© The Author(s) 2022